Inverter-Less Hybrid Voltage/Var Control for Distribution Circuits With Photovoltaic Generators

Zhaoyu Wang, *Student Member, IEEE*, Hao Chen, *Student Member, IEEE*, Jianhui Wang, *Senior Member, IEEE*, and Miroslav Begovic, *Fellow, IEEE*

***Abstract*—This paper proposes a hybrid voltage/var control (VVC) architecture for distribution systems with a high PV penetration. The architecture consists of two control loops: coordinated normal control loop and uncoordinated transient cloud movement control loop. In the first loop, hourly dispatches are scheduled for on-load tap changer (OLTC), capacitor banks (CBs), and static var compensators (SVCs) based on forecasted load and PV power output so as to minimize power losses and voltage deviations. The second loop is triggered when large variations of PV power output caused by rapid cloud movement happen. All SVCs and CBs become self-controlled based on local voltage measurements with the single control objective to minimize voltage deviations. SVCs will operate firstly to flatten the voltage profile. If SVCs fail, CBs will switch to provide reactive power support. A time-adaptive delay is applied to each CB to avoid overcompensation. Case studies show the proposed method can optimize the system operation and is effective in voltage regulation with PV generators.**

***Index Terms*—Distributed generators, distribution systems, photovoltaic (PV) generation, reactive power control, voltage control.**

I. Nomenclature

P_i	Active power flow from node i to $i+1$.
Q_i	Reactive power flow from node i to $i+1$.
V_i	Voltage at node i.
δV_i	Voltage deviation between V_i and V_0.
$p_{i,l}$	Active load consumption at node i.
$q_{i,l}$	Reactive load consumption at node i.
$p_{i,g}$	Active power generation at node i.
$q_{i,g}$	Reactive power generation at node i.
$q_{i,g}^{\max}$	Maximum reactive power generation at node i.
$r_i + jx_i$	Impedance of the line between nodes i and $i+1$.
ℓ	Active system power losses.
λ	Maximum voltage deviation along the feeder.
$c_{ik,t}$	Binary indicator of switch status of kth capacitor in the capacitor bank (CB) at node i (1-ON, 0-OFF) at time t.
$a_{ik,t}$	Binary indicator $a_{ik,t} = c_{ik,t}c_{ik,t+1}$.
$s_{ik,t}$	Binary indicator for switch status change of the k th capacitor in the CB at node i from time t to $t+1$.
$\mathrm{CAP}_{ik}^{\max}$	Maximum daily number of operations of kth capacitor in the CB at node i.
β_t	Integer representing tap changes of the OLTC from time t to $t+1$.
$\mathrm{TAP}^{\max}$	Maximum daily number of OLTC operations.
b_{is}	Binary indicator of sth output value of the SVC at node i (1-select, 0-not select).
q_i^{svcs}	sth output value of SVC at node i.
$q_i^{\mathrm{cap}k}$	Size of kth capacitor of the CB at node i.
V_i^{ref}	Reference voltage at node i.
ς	Maximum allowable voltage deviation in the transient cloud movement control loop.
ε_i	Voltage deviation between V_i^{ref} and V_i.
TD_i	Operation time delay of CB at node i.
K_i	Time gain of CB at node i.
α_i	Time exponent of CB at node i.
η	PV power output change (kw/s).
T	Time horizon (e.g., 24 h).

Manuscript received September 21, 2013; revised January 13, 2014, March 13, 2014; accepted April 20, 2014. Date of publication September 10, 2014; date of current version October 17, 2014. Paper no. TSG-00744-2013.

Z. Wang, H. Chen and M. Begovic are with the Georgia Institute of Technology, Atlanta, GA 30332 USA (e-mail: zhaoyuwang@gatech.edu, hchen95@gatech.edu, miroslav@ece.gatech.edu).

J. Wang is with Argonne National Laboratory, Lemont, IL 60439 USA (e-mail: jianhui.wang@anl.gov).

Color versions of one or more of the figures in this paper are available online at http://ieeexplore.ieee.org.

Digital Object Identifier 10.1109/TSG.2014.2324569

II. Introduction

VOLTAGE AND var control (VVC) is critical to distribution systems since a proper dispatch of VVC devices can improve power quality and reduce power losses. The increasing penetration of photovoltaic generators (PV) has greatly influenced conventional VVC due to the highly variable outputs of PV.

VVC can be categorized as uncoordinated vs. coordinated [1]. Uncoordinated VVC operates VVC devices such as on-load tap changer (OLTC), capacitor banks (CBs), and fast-responding voltage regulators locally to maintain the voltage along the feeder within an acceptable range. The advantages of this method include its simplicity and quick response to disturbances. The drawbacks are that power losses

are not taken into account and the operation of the system may not be optimal. In coordinated control, a centralized optimization algorithm makes dispatch decisions for each VVC device based on forecasted load and generation. The advantage is that a multi-objective optimal control of the system may be achieved. The drawbacks are its complexity and inability to respond to load or generation ramps promptly. Coordinated VVC is well studied in the literature [2]–[6]. In [2], OLTC and capacitors are dispatched hourly based on one-day ahead load forecast. The study in [3] proposes a two-stage coordinated control scheme between OLTC and CBs. The dispatch schedule of CBs is generated using genetic algorithm (GA) based on forecasted load, and the OLTC is controlled in real time. The study in [4] coordinates the control of OLTC and static var compensators (SVCs) in a distribution system. However, none of them considers the existence of PV.

As the penetration level of PV grows, their impacts on voltage and reactive power in distribution systems have attracted increasing attention around the world [7], [8]. The output of PV can be highly variable and ramp up on the order of 15% of its capacity per minute with intermittent cloud coverage [9]. The small X/R ratio of distribution circuits highlights impacts of could effects on VVC [10]. It is reported by [11] that the transient cloud movement may cause voltage fluctuation problems when the PV penetration exceeds 20%. During these periods, the solar radiation can change as quickly as 705 W/m^2/s, and it only takes a few seconds for a clear sky to change to be heavily cloudy [12]. Many techniques have been developed to deal with the variable nature of PV generation. Reference [13] uses energy-storage devices to manage PV variations. But the costs of energy-storage devices are too high to be widely implemented in practice. In [10], the stochastic nature of distributed generation is taken into account to schedule VVC dispatch, but the transient cloud movement effects of PV are not considered.

Using PV inverters to provide reactive power support during the transient cloud movement period has drawn more attention in recent years [12], [14]–[18]. Study in [16] proposes a two time-scale optimal control scheme. CBs are controlled in a slow time scale, while PV inverters are controlled on a fast time scale. Reference [17] designs an algorithm to balance the need of flattening voltage profile with the desire to minimize losses. PV inverters are controlled based on the balancing algorithm and instantaneous measurements. The algorithms proposed in [16] and [17] require complex communications. The latency in communication and the optimization algorithms may slow down algorithm performances during rapid changes in cloud coverage [14]. Reference [12] analyzes the impacts of cloud effects on voltage stability and finds that reactive power support provided by PV inverters can solve the instability problem. Reference [18] proposes a two-stage local control architecture to realize VVC. Inverters provide reactive power support when the demand is small. In comparison, both inverters and CBs will react if the demand is large. The VVC is based on local controllers, which can provide rapid response to voltage violations. However, there are no time delays assumed for the operations of VVC devices, which may cause overcompensation problems. In general, although new IEEE standards are trying to relieve constraints on PV integrations [19], there could be some potential drawbacks of using PV inverters to provide reactive power support: 1) injecting reactive power by PV inverters is not widely accepted by utilities currently and IEEE Std. 1547, which recommends PV to be operated at a unity power factor is still the effective standard for utility practices [20], [21]; 2) more expensive oversized inverters are needed; 3) generating reactive power will decrease the profits of PV owners; 4) the coordination among inverters and between inverters and other VVC devices is not clear; 5) further research on the night-mode operation of inverters is still necessary [22]. Hence, we only propose to use the existing voltage/var control devices that are most widely available in practice in this paper.

TABLE I
TIMESCALES OF ACTION

Device	OLTC	CB [26-28]	SVC [29]
Timescale	sec. to min.	1-2 cycles	half cycle

In this paper, a new hybrid VVC scheme is proposed to realize the optimal control of the distribution systems while effectively dealing with the voltage regulation problem of PV caused by fast cloud movement. Compared with previous methods, the proposed technique relies on OLTC, CBs, and static var systems (SVS) to achieve VVC on feeders with a high PV penetration without violating the current IEEE PV integration standards or requiring resizing of the inverters. The SVS can be SVCs or distribution STATCOMs (DSTATCOMs) [23], [24]. In this paper, it is assumed that SVCs exist in the feeder. The proposed method can also cooperate with overvoltage controllers [25] to further alleviate voltage rise due to PV integrations. Thus, the proposed method is a practical and economic way to be implemented in distribution systems with PV generators.

There are two loops in the proposed control scheme: coordinated normal control loop and uncoordinated transient cloud movement control loop. The normal control loop makes hourly dispatch schedules for OLTC, CBs, and SVCs based on forecasted load and PV power output. The control objective is to minimize power losses and voltage deviations. When clouds move over, the variations of PV power output will trigger the uncoordinated control loop. All SVCs and CBs become self-controlled based on local voltage measurements. Each SVC or CB is assigned a reference voltage V_i^{ref}. The only control objective is to maintain the deviation between the node voltage and its reference voltage within a predefined range. Since there is no communication or optimal coordination in the second control loop, it can respond quickly to transient cloud effects. Table I shows the timescales of actions of OLTC, SVCs, and CBs. If the distribution system is equipped with DSTATCOMs, the DSTATCOMs can perform the functions of SVCs in the transient cloud movement control loop.

The remainder of this paper is organized as follows. Section III introduces the distribution system model and the proposed hybrid VVC architecture. Section IV discusses three case studies to show the effectiveness of the proposed method. Section V concludes the paper with major findings.

III. HYBRID VOLTAGE/VAR CONTROL ARCHITECTURE

A. Distribution System Model

Consider a distribution system as shown in Fig. 1, there are n buses indexed by $i = 0, 1, \ldots, n$. DistFlow [17], [30] equations can be used to describe the complex power flows at each node i.

$$P_{i+1} = P_i - r_i \frac{P_i^2 + Q_i^2}{V_i^2} - p_{i+1} \tag{1}$$

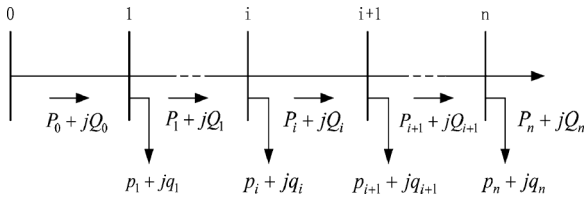

Fig. 1. Schematic diagram of a radial distribution system.

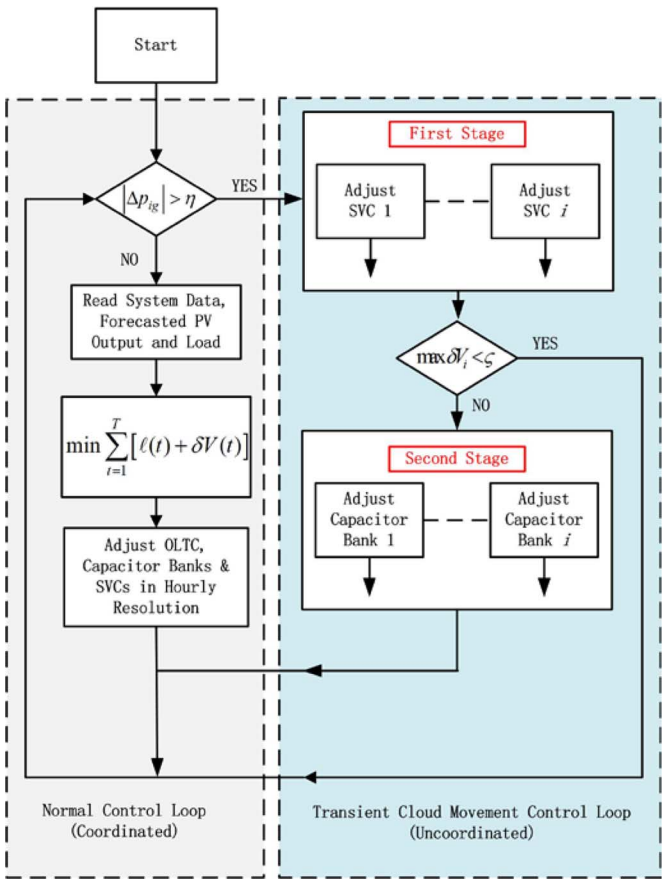

Fig. 2. Flowchart of the proposed control strategy.

$$Q_{i+1} = Q_i - x_i \frac{P_i^2 + Q_i^2}{V_i^2} - q_{i+1} \tag{2}$$

$$V_{i+1}^2 = V_i^2 - 2(r_i P_i + x_i Q_i) + (r_i^2 + x_i^2)\frac{P_i^2 + Q_i^2}{V_i^2} \tag{3}$$

$$p_i = p_{i,l} - p_{i,g}, q_i = q_{i,l} - q_{i,g} \tag{4}$$

In (4), $p_{i,g}$ is the active power generated by DG units which are PV generators at node i in this paper, $q_{i,g}$ is generated by var compensation devices such as CBs or SVCs at node i.

Fig. 2 shows the flowchart of the proposed hybrid VVC control architecture. There are three VVC devices to be controlled: OLTC, CBs and SVCs. Each CB is composed of several small capacitors that can switch on/off individually. There are two advantages to use small capacitor-based CBs: 1) the average number of switching each small capacitor can be reduced; 2) it is possible to adjust the CB output in a discrete manner with small increments/decrements. In comparison, SVCs can be controlled continuously or discretely. The discrete control of SVCs is more popular in practical systems and considered in this paper due to its lower cost and absence of harmonic injections [31].

The overall control strategy proposed in this paper can be divided into two parts: normal control loop and transient cloud movement control loop. The normal control loop coordinates the OLTC, CBs, and SVCs to achieve the multi-objective optimal operation of the circuits. The transient cloud movement control loop becomes effective when the output of PV generators changes significantly due to intermittent cloud coverage. In order to react fast to the moving clouds, uncoordinated controls of SVCs and CBs are applied to achieve a single control objective: to maintain the voltage along the feeder within the predefined range. The SVCs and CBs in the transient cloud movement loop are self-controlled without any coordination. The switching times of all small capacitors in CBs are continuously updated to make sure that they are lower than the maximum values. Details of the two control loops are discussed in the following subsections.

B. Normal Control Loop: Optimal Coordinated Control

When there is no or less cloud coverage, the VVC devices will be controlled by the normal loop. Optimal coordinated control requires communication among measurement devices, VVC devices and the centralized optimization algorithm. Moreover, for a system with a m-step OLTC and n capacitors, there will be $m \times 2^n$ possible states for dispatch, which requires a large computational effort. Although capacitors can be switched quickly after receiving control signals, the communication between the central controller and CBs takes longer time. Meanwhile, the action of OLTC also needs some time. Thus, the coordinated control is on a slower timescale such as hourly. In this paper, one day is divided into twenty-four time slots. The optimal dispatch decisions are made and sent to each VVC device for each time slot based on the forecasted load and PV power output. Please note the proposed normal control loop can also be used hours ahead in real time or sub-hourly as long as the forecasts for the time intervals are available and the devices can act quickly enough.

Consider using power losses of the distribution system and voltage deviations along the feeder as control objectives, the multi-objective optimal control problem for one day can be formulated as follows:

$$\min \sum_{t=1}^{T} [\ell(t) + \delta V(t)] \tag{5}$$

subject to

$$\delta V(t) = \max \delta V_i(t), \delta V_i(t) = |V_i(t) - V_0(t)|, i = 1, \ldots, n \tag{6}$$

$$\ell(t) = \sum_{i=0}^{n} r_i \frac{P_i^2(t) + Q_i^2(t)}{V_0^2(t)} \tag{7}$$

$$P_{i+1}(t) = P_i(t) - p_{i+1}(t) \tag{8}$$

$$Q_{i+1}(t) = Q_i(t) - q_{i+1}(t) \tag{9}$$

$$V_{i+1}(t) = V_i(t) - \frac{r_i P_i(t) + x_i Q_i(t)}{V_0(t)} \tag{10}$$

$$p_i(t) = p_{i,l}(t) - p_{i,g}(t), q_i(t) = q_{i,l}(t) - q_{i,g}(t) \tag{11}$$

$$V_i^{\min} \le V_i(t) \le V_i^{\max} \tag{12}$$

$$0 \le q_{i,g}(t) \le q_{i,g}^{\max} \tag{13}$$

$$V_0(t) = \mathrm{TAP}_t V_s \tag{14}$$

TABLE II
THE RELATIONSHIP AMONG $s_{ik,t}, a_{ik,t}$ AND $c_{ik,t}$

$s_{ik,t}$	$a_{ik,t}$	$c_{ik,t+1}$	$c_{ik,t}$
0	0	0	0
0	1	1	1
1	0	0	1
1	0	1	0

$$\sum_t |c_{ik,t+1} - c_{ik,t}| \le \mathrm{CAP}_{ik}^{\max} \tag{15}$$

$$\sum_t |\mathrm{TAP}_{t+1} - \mathrm{TAP}_t| \le \mathrm{TAP}^{\max} \tag{16}$$

In constraint (6), V_0 is the secondary voltage of the substation transformer. Constraint (7) represents the power losses along the entire distribution feeder. Equations (8)–(10) are the linear form of the DistFlow equations defined in (1)–(4), which has been extensively verified and used in the literature [9], [17], [30], [32]. The linearization is based on the facts that nonlinear terms in (1)–(4) are much smaller than linear terms [9], [30]. In (11), outputs of DGs and var compensation devices are represented as negative active and reactive loads, respectively. Equation (12) represents the permissible voltage ranges of all nodes (usually from 0.95 p.u. to 1.05 p.u.). In constraint (14), V_s represents the primary voltage of the transformer at the substation, which is assumed to be 1.0 p.u. in this paper. The daily switch times of capacitors and OLTC, which are describes in (15) and (16) should be less than predefined maximum values. For (6), it is necessary to remove the absolute value so as to reduce the non-linearity of the original formulation. Thus, (6) can be reformulated as (17). One of (17a) and (17b) is redundant, depending on the magnitude of $V_0(t)$ and $V_i(t)$.

$$\lambda(t) \ge V_i(t) - V_0(t), \forall i \tag{17a}$$

$$\lambda(t) \ge V_0(t) - V_i(t), \forall i \tag{17b}$$

In constraint (15), assuming $s_{ik,t} = (c_{ik,t+1} - c_{ik,t})^2$, since $c_{ik,t}$ is a binary, $c_{ik,t}^2 = c_{ik,t}$, we have

$$s_{ik,t} = c_{ik,t+1} + c_{ik,t} - 2c_{ik,t+1}c_{ik,t} \tag{18}$$

$s_{ik,t}$ indicates whether the k th capacitor at node i has changed its status from time t to time $t+1$ ($s_{ik,t} = 1$, if the status has changed). To linearize the multiplication of $c_{ik,t+1}c_{ik,t}$, we denote $a_{ik,t} = c_{ik,t+1}c_{ik,t}$ and $a_{ik,t}$ is a binary. Equation (22) can be represented as (23)–(24).

$$s_{ik,t} = c_{ik,t+1} + c_{ik,t} - 2a_{ik,t} \tag{19}$$

$$a_{ik,t} \le c_{ik,t}, a_{ik,t} \le c_{ik,t+1}, a_{ik,t} \ge c_{ik,t} + c_{ik,t+1} - 1 \tag{20}$$

Table II illustrates the effectiveness of (19) and (20). It can be seen that $s_{ik,t}$ can represent the switch status of the capacitor. The constraint (15) can be reformulated as a linear constraint:

$$\sum_t s_{ik,t} = \sum_t (c_{ik,t+1} + c_{ik,t} - 2a_{ik,t}) \le \mathrm{CAP}_{ik}^{\max} \tag{21}$$

In constraint (16), TAP_t is an integer whose range is dependent on the number of taps of the OLTC. Equation (16) can be reformulated as follows:

$$\beta_t \ge \mathrm{TAP}_{t+1} - \mathrm{TAP}_t \tag{22a}$$

$$\beta_t \ge \mathrm{TAP}_t - \mathrm{TAP}_{t+1} \tag{22b}$$

$$\sum_t \beta_t \le \mathrm{TAP}^{\max} \tag{22c}$$

For nodes without PV, $p_{i,g} = 0$; for those with PV, p_{ig} cannot be dispatched, but can be forecasted. For nodes without var compensation, $q_{i,g} = 0$. For those with SVCs, $q_{i,g}$ can be selected from a set of discrete values since SVCs are assumed to be controlled discretely as shown below:

$$q_{i,g}(t) = b_{i1}(t)q_i^{\mathrm{svc1}} + b_{i2}(t)q_i^{\mathrm{svc2}} + \cdots + b_{\mathrm{is}}(t)q_i^{\mathrm{svcz}}$$
$$\sum_{s=1}^{z} b_{\mathrm{is}}(t) = 1 \tag{23}$$

For nodes with CBs, $q_{i,g}$ can be expressed as a combination of outputs of capacitors in the CB.

$$q_{i,g}(t) = \mathrm{CAP}_{i1}(t)q_i^{\mathrm{cap1}} + \mathrm{CAP}_{i2}(t)q_i^{\mathrm{cap2}} + \cdots + \mathrm{CAP}_{ik}(t)q_i^{\mathrm{capk}} \tag{24}$$

The above formulation schedules the dispatches of VVC devices for each time interval based on the forecasted load and PV power output so as to minimize active power losses and voltage deviations. The problem is a mix-integer programming (MIP) problem, which can be solved by GAMS. However, due to the longer time required for computation, communication and mechanical action, the proposed normal control loop may be still too slow to respond to transient cloud movement.

C. Transient Cloud Movement Control Loop: Local Control by SVCs and Capacitors

As shown in Fig. 1, the voltage drop between node $i-1$ and i can be approximated as follows [1]:

$$\Delta V_{i,i+1} = V_i - V_{i+1} \approx \frac{r_i(P_i + p_{i,l} - p_{i,g}) + x_i(Q_i + q_{i,l} - q_{i,g})}{V_{i+1}} \tag{25}$$

Solar radiation changes quickly when cloud coverage varies, which will result in sharp fluctuations of PV output. If $p_{i,g}$ decreases, the voltage drop between two nodes will increase. In this circumstance, $q_{i,g}$ should increase fast to provide enough reactive power compensation to flatten the voltage profile. As shown in Fig. 3, the drop of PV output $\Delta p_{i,g}$ triggers the transient cloud movement control loop, in which, SVCs and CBs are self-controlled without any communication or coordination to minimize the voltage deviation at each node. By using decentralized control, SVCs and CBs can generate quick responses to transient cloud effects.

There are two stages in the transient cloud movement control loop. In the first stage, only SVCs are used to regulate voltage while additional CBs will be used in the second stage to provide more reactive power support. There two reasons why SVCs are included in the first stage: 1) the action of SVCs is faster; 2) if the cloud is not severe, SVCs can regulate the voltage, there is no need to use capacitors, which can reduce the switches of capacitors. As discussed in the introduction, the control objective is to minimize ε_i at each node. ε_i might be different from δV_i, if V_i^{ref} is not equal to V_0.

$$\varepsilon_i = \left| V_i^{\mathrm{ref}} - V_i \right| \tag{26}$$

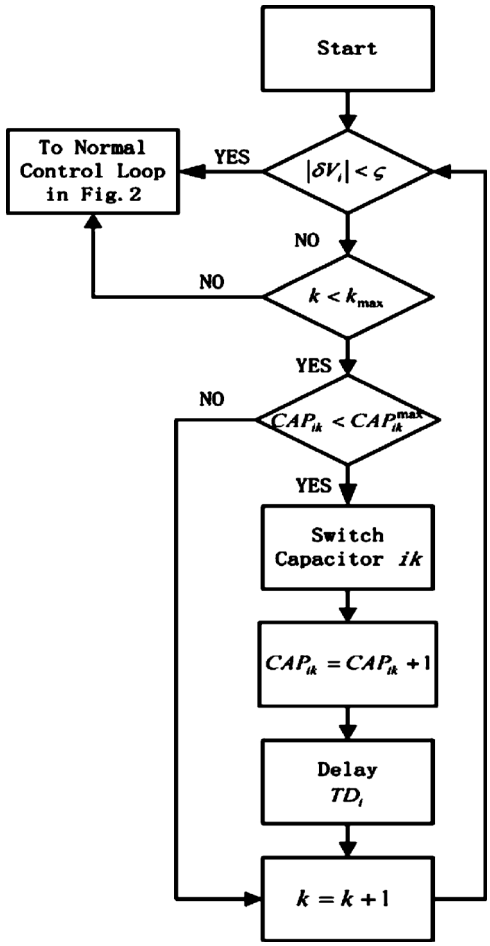

Fig. 3. Second-stage control flowchart for the capacitor bank at node i in transient cloud movement control group.

In the flowchart shown in Fig. 2, SVCs will begin to regulate voltage in the uncoordinated control model in the first stage as long as the voltage deviation, ε_i, is small enough. A SVC is able to adjust its output susceptance based on local measurements to regulate the voltage of the local node to be close to a reference voltage (a detailed description of SVCs can be found in [31], [33]). If the cloud effect is not severe, the voltage profile should be flattened by SVCs, which means the control system can return to the normal loop without entering the second stage. However, if the cloud effect is severe and SVCs cannot provide enough reactive power support, the control system will enter the second stage to trigger the local control of CBs.

In the second stage, each CB only monitors the voltage at its installed node and makes decisions by itself without any communication with the other CBs, which can ensure its quick response. The lower part of Fig. 3 shows the proposed local control flowchart of a CB during a severe transient cloud movement period. Capacitors will be switched until the voltage deviation is within the pre-defined range or the maximum number of operations is reached. Since capacitors detect voltage deviations at the same time, all of them will be switched if there is no time delay, which may cause overcompensation of reactive power and large voltage swings.

The desired response of the capacitor bank at node i can be described as [34]:

$$q_{i,g}(t) = q_{i,g}^{F} - \left(q_{i,g}^{F} - q_{i,g}^{0}\right) e^{-t/\tau} \tag{27}$$

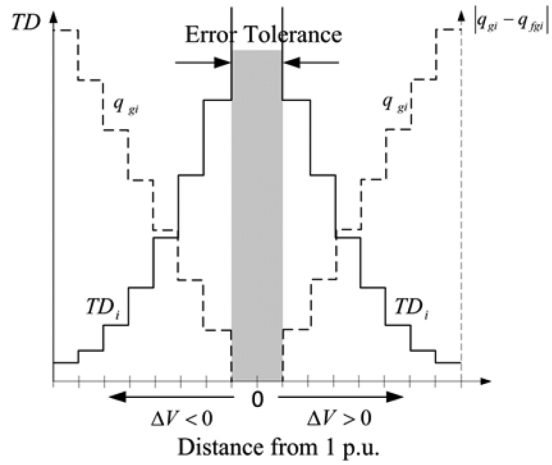

Fig. 4. CB output with adaptive time delay.

where $q_{i,g}^{F}$ is the final value of the reactive power required by the system from the capacitor bank (CB), and $q_{i,g}^{0}$ is the initial amount of reactive power presently being injected. τ is a time constant which determines the injection rate of the reactive power. The time constant can be calculated based on the difference between the reference voltage and the measured voltage. A capacitor bank is composed of several capacitors. Therefore, we assume the reactive power injected by a capacitor bank at a given time interval is discrete and constrained to a fixed value which is the size of a single capacitor in the CB, while the injection time interval is varied. The time interval should be continuously updated, as changes in loads, sources, and the injection levels of adjacent capacitor banks may change the grid voltage.

Thus, a time delay TD_i is added to every CB to enable CBs to be switched in turn. For a certain CB at node i, TD_i is time-adaptive, which means TD_i is updated after the operation of the previous capacitors in this CB as shown in the following equation.

$$\mathrm{TD}_i = K_i \left|V_i^{\mathrm{ref}} - V_i\right|^{\alpha_i} \tag{28}$$

K_i and α_i can be used to control the range of time delay. K_i is a positive value and α_i is a negative value. Larger absolute values of K_i and α_i can result in longer time delay. In this paper, we assume K_i equals 1 and α_i equals -1.

Fig. 4 shows the output of a certain CB installed at node i. When the voltage deviation from the reference voltage at node i becomes larger, TD_i becomes smaller and capacitors can operate faster; when V_i is approaching V_{ref}, TD_i becomes larger, which indicates additional CBs may not be switched immediately and only need to be switched if the voltage deviation still exists. Since only one capacitor in the CB is switched at each time, Δq is a fixed value which is equal to the size of the switched capacitor in the CB, and the output of the CB increases discretely. As there is no communication among CBs, each CB does not know the operations of other CBs. After one capacitor is switched, the CB becomes idle for a period of TD_i to check whether the nodal voltage is fully recovered. If the nodal voltage is still out of range, another capacitor in this CB will be switched. When the voltage deviation at the CB node is within the range, the current CB will return to the normal control loop. For a system without SVCs, the first stage of the transient cloud movement control loop does not exist. However, the second

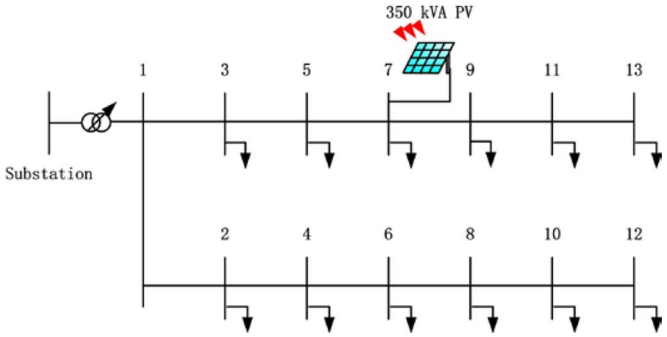

Fig. 5. Test distribution sytem.

stage of the control loop can still work with capacitor banks to regulate the voltage as shown in Fig. 3.

In sum, the advantages of the proposed transient cloud movement control loop can be summarized as follows:

- A simple structure suitable for decentralized control of multiple units.
- More stable operation as a result of the adaptive time delay.

IV. Case Study

A. Two-Feeder Test System

This section presents simulation results of three cases: coordinated normal control, uncoordinated transient cloud movement control by SVCs and uncoordinated control by SVCs and CBs. Fig. 5 shows the two-feeder test distribution system, the details can be found in Appendix. The base MVA is 1.5 MVA. We assume a PV generator is connected to node 7 on the primary feeder.

The proposed control framework can also be extended to the case where multiple PV generators are connected to different nodes on the system without loss of generality, as the problem formulation in the normal control loop remains the same, and the uncoordinated control loop can still work well since it only relies on local voltage measurements. Meanwhile, the proposed method can be applied to distribution systems with more nodes; the only difference is that the search space for the optimal solution in the normal control loop might become larger. The substation transformer is with $\pm 5\%$ tap range and 10 tap positions. There are two SVCs installed on the primary feeder, one is at node 5, the other is at node 11. The maximum output of each SVC is 26 kVar. CBs are installed at nodes 3, 7, 9 and 13 of the primary feeder, and at nodes 4 and 10 of the secondary feeder. For each CB, $\Delta q = 1$ kVar and the maximum output is 30 kVar. We also assume $\eta = 25$ kW/s and $\varsigma = 0.01$ p.u.

1) Case 1: This case demonstrates how the coordinated normal control loop works based on the forecasted load and PV output as shown in Fig. 6. The data for forecasted PV output can be found in [35]. The PV output is hourly averaged data, in which, the rapid fluctuations caused by cloud effects are not included since the coordinated control works on an hourly resolution. Cases 2 and 3 will discuss how to deal with the transient cloud effects in the uncoordinated control loop below.

Based on the forecasted load and PV output as well as the formulation of (5)–(24), the optimal dispatch of VVC devices can be achieved. For illustration, the optimal dispatch between 08:00 AM to 11:00 AM is discussed in this case. The optimal

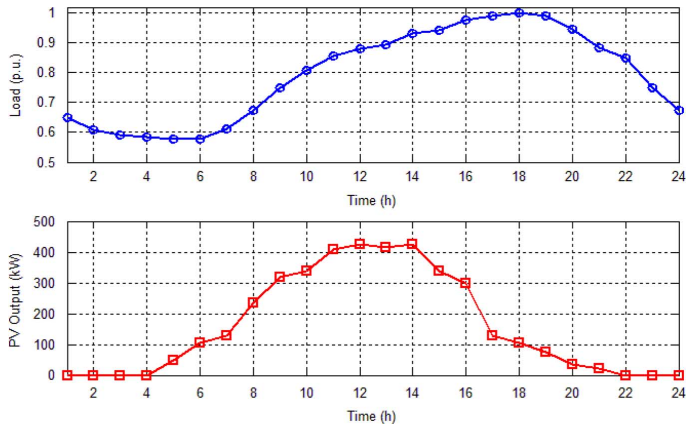

Fig. 6. Forecasted load and PV output.

TABLE III
VVC Dispatch From 08:00 AM to 11:00 AM

Time	Tap	q3 (kVar)	q5 (kVar)	q7 (kVar)	q9 (kVar)
08:00	-1	23	21	19	19
		q11(kVar)	q13 (kVar)	q4 (kVar)	q10 (kVar)
		18	18	26	28
09:00	0	q3 (kVar)	q5 (kVar)	q7 (kVar)	q9 (kVar)
		26	22	19	18
		q11(kVar)	q13 (kVar)	q4 (kVar)	q10 (kVar)
		17	16	26	28
10:00	0	q3 (kVar)	q5 (kVar)	q7 (kVar)	q9 (kVar)
		27	24	16	16
		q11(kVar)	q13 (kVar)	q4 (kVar)	q10 (kVar)
		14	14	27	28
11:00	0	q3 (kVar)	q5 (kVar)	q7 (kVar)	q9 (kVar)
		27	25	16	16
		q11(kVar)	q13 (kVar)	q4 (kVar)	q10 (kVar)
		14	14	28	28

solutions of the VVC dispatch are in hourly solution. The optimization results are shown in Table III.

When there is enough solar radiation, PV generators can support the voltage and reduce the need for var compensation. As shown in Table III, the outputs of CBs on the primary feeder are much lower than those on the secondary feeder since there is no PV connected with the secondary feeder. Meanwhile, as load changes by about 8% from 10:00 AM to 11:00 AM, the outputs of CBs and SVCs do not change too much and the var compensation at nodes 7, 9, 11 and 13 remain the same. During the same period, the PV output increases by 20%, from 340 kw to 408 kw. According to (25), because the load increase is compensated by the increasing output of the PV generator, the voltage deviation does not become larger.

Fig. 7 shows the maximum voltage deviations of all nodes from 8:00 AM to 11:00 AM with and without VVC. It can be seen that the voltage deviations are reduced by around 40% through the implementation of the proposed VVC algorithm.

Fig. 8 shows the active power losses of the system. Applying VVC to the system can reduce active power losses by around 20%.

2) Case 2: Case 2 demonstrates the first stage of the uncoordinated transient cloud movement control loop. As shown in Fig. 9, we assume clouds move over after 5 s and the output of PV generation decreases from 300 kW to 200 kW. SVCs

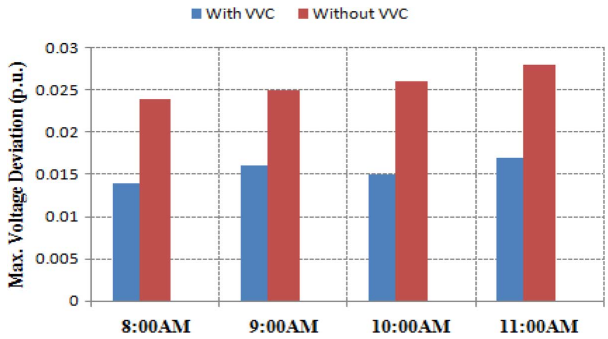

Fig. 7. Max voltage deviations with and without VVC.

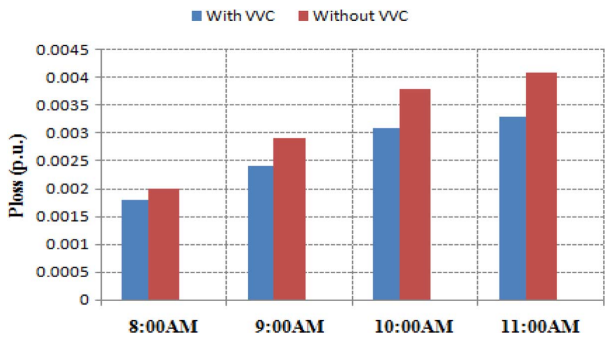

Fig. 8. Power losses with and without VVC.

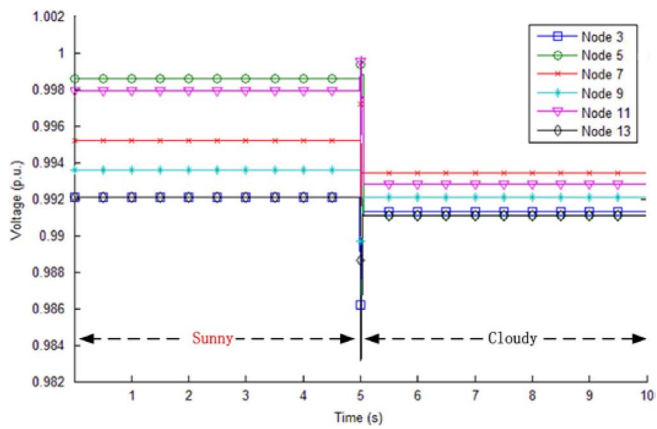

Fig. 9. Voltage profile of primary feeder.

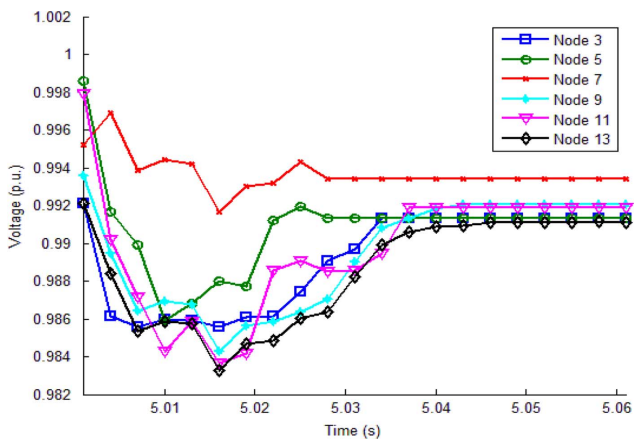

Fig. 10. Zoomed-in voltage profile of primary feeder.

become locally controlled to provide reactive power support. Fig. 10 is a zoomed-in plot of Fig. 9, which shows the detailed changes of voltages.

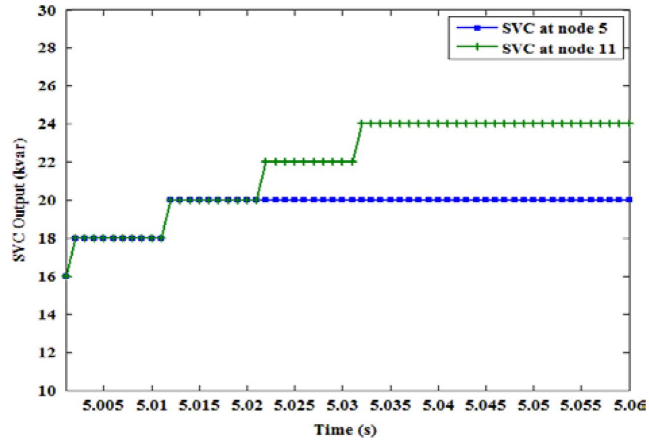

Fig. 11. Outputs of SVCs.

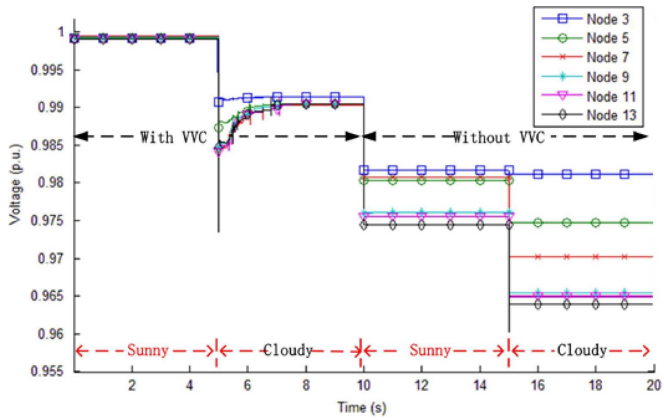

Fig. 12. Voltage profile of primary feeder.

Fig. 11 shows the outputs of SVCs at node 5 and node 11. It can be seen that SVCs start increasing outputs in a discrete manner after the rapid change of solar radiation and voltage drop. When the voltage deviations of all nodes are within 1% of the substation voltage at about 5.04 s, SVCs stop injecting reactive power. The outputs of both SVCs are at their maximum. Thus, SVCs are capable of dealing with the current cloud effect, the control returns to the coordinated normal loop.

3) Case 3: In Case 3, a more severe transient cloud effect is simulated. As shown in Fig. 12, the first 10-second plot shows the voltage profile of the primary feeder when the proposed VVC is applied. The plot of 11 to 20 seconds represents the voltage profile without VVC. Severe cloud effects start after 5 s from the start of the simulation. The output of PV generation decreases from 300 kW to 50 kW. Fig. 13 is a zoomed-in plot of Fig. 12, which shows the detailed changes of voltages with VVC during the transient cloud movement.

As shown in Fig. 14, SVCs operate firstly to provide reactive power support. It can be seen from Figs. 12 and 13 that the voltage deviations are still larger than 1% after both SVCs reach their maximum outputs. Thus, VVC enters the second stage of the uncoordinated control loop. CBs become locally controlled. All CBs start generating more reactive power, only one capacitor in each CB is switched at one time, so the outputs of CBs increase in a discrete manner. Since there is no communication among CBs, and each CB is self-controlled with its own time-adaptive delay, it is possible that capacitors of different CBs are switched at the same time. Considering the small sizes

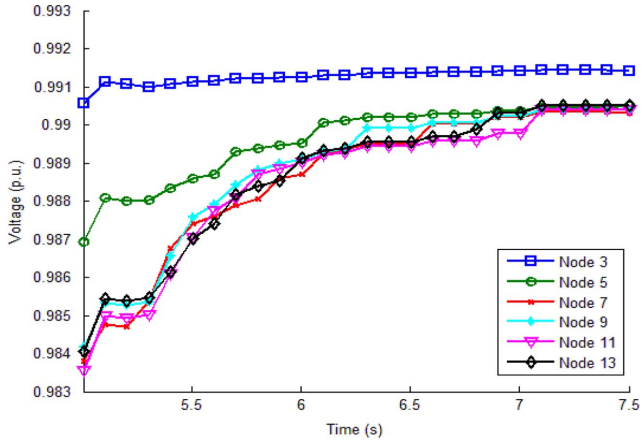

Fig. 13. Zoomed-in voltage profile of primary feeder.

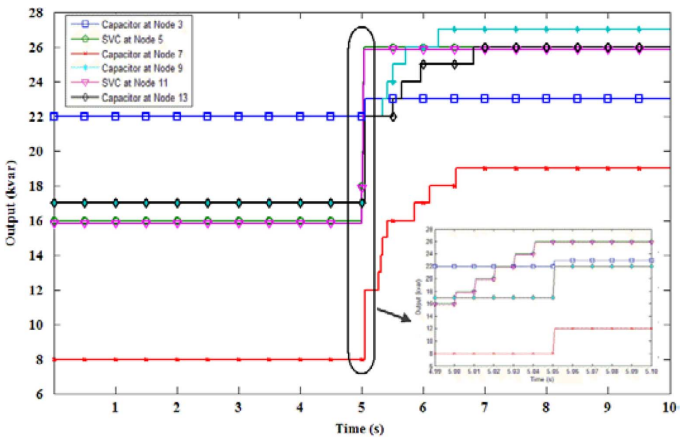

Fig. 14. Output of SVCs and CBs.

of capacitors and the variable time-delays, there will be no over-compensation problem with the proposed algorithm. Take the CB at node 7 as an example, the output increases fast when the voltage deviation is large; after the nodal voltage is close to the range, the time delay becomes larger and the output increases slower until the nodal voltage deviation is within the range.

Fig. 12 also shows what the voltage profile would be if there is no VVC. It is assumed that it is sunny between 10 s to 15 s and clouds move over at 15 s. It can be seen that system voltages are much lower after 15 s and more vulnerable to cloud effects than those with the proposed VVC architecture. Reference [36] studied the centralized coordination control between OLTC and SVCs for voltage regulation in a distribution system with PV generators. It takes several minutes to generate control signals and regulate voltage levels when the fast moving clouds effects happen [36]. However, the proposed decentralized method in this paper can restore the voltage level to a desired value within a few seconds during the transient cloud movement as shown in Figs. 12 and 13. Hence, the proposed method is more efficient in terms of shorter response time.

B. IEEE 123-Bus Test System

The modified IEEE 123-bus test system is considered. The network parameters and load data can be obtained from [37]. The base MVA is 10 MVA. Fig. 15 shows the topology of the test system. We assume PV panels are connected to nodes 13 and 60, each is 500 kVA. The substation transformer is with $\pm 5\%$ tap range and 10 tap positions. Two SVCs are installed at

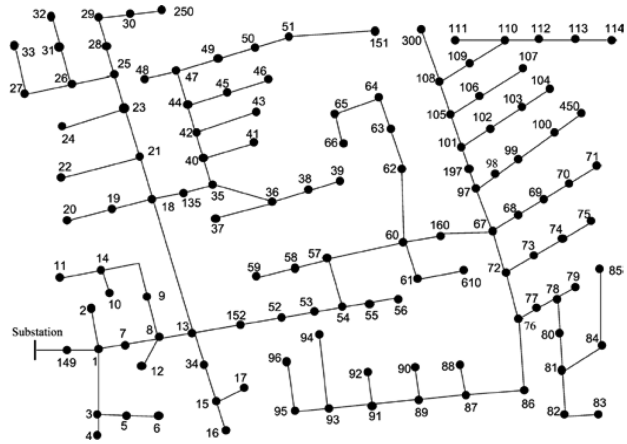

Fig. 15. IEEE 123-Bus Test System.

TABLE IV
VVC DISPATCH FROM 10:00 TO 13:00

Time	Tap	q18(kVar)	q44(kVar)	q57(kVar)
10:00	0	30	21	33
		q67(kVar)	q86(kVar)	q109(kVar)
		22	21	14
11:00	0	q18(kVar)	q44(kVar)	q57(kVar)
		31	21	32
		q67(kVar)	q86(kVar)	q109(kVar)
		22	20	14
12:00	-1	q18(kVar)	q44(kVar)	q57(kVar)
		31	20	32
		q67(kVar)	q86(kVar)	q109(kVar)
		21	19	13
13:00	0	q18(kVar)	q44(kVar)	q57(kVar)
		32	20	31
		q67(kVar)	q86(kVar)	q109(kVar)
		22	21	14

nodes 18 and 57, each is 40 kVar. Capacitor banks are installed at nodes 44, 67, 86, and 109. For each CB, $\Delta q = 1$ kVar and the maximum output is 30 kVar. It is also assumed that $\eta = 25$ kW/s and $\varsigma = 0.01$ p.u.

It is assumed that the forecasted load and PV output profiles are the same as shown in Fig. 6. The optimal dispatch of VVC devices can be achieved by solving the formulation of (5)–(24). For illustration, the hourly optimal dispatch between 10:00 to 13:00 is shown in Table IV. The maximum voltage deviations are 0.019 p.u. with VVC and 0.042 p.u. without VVC. The averaged active power losses during this period are 0.012 p.u. with VVC and 0.019 p.u. without VVC. It can be seen that the voltage deviations are reduced by around 55% and the active power losses are reduced by around 36% through the implementation of the proposed VVC algorithm.

Assume a moderate change of PV generation happens at 13:00. The outputs of the two PV generators decrease from 400 kW to 300 kW. Fig. 16 shows the outputs of SVCs at node 18 and node 57. Fig. 17 shows the minimum voltage in the test system. It can be seen that SVCs start increasing outputs after the rapid change of solar radiation and voltage drop. When the voltage deviations of all nodes are within 1% of the substation voltage at about 5.04 s, SVCs stop injecting reactive power.

To test the performance of the proposed control method during a severe cloud movement, we assume a more severe change of PV generation happens at 13:00. The outputs of the

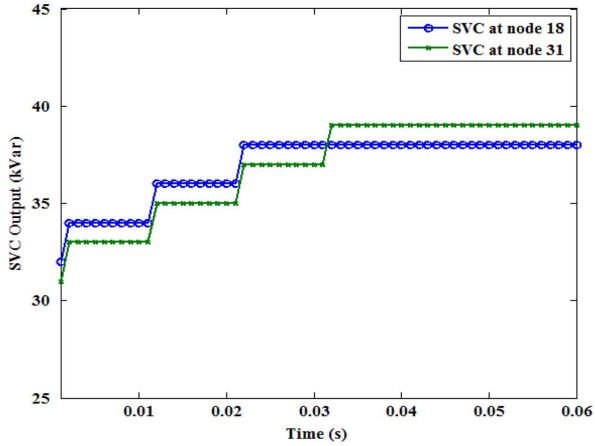

Fig. 16. Outputs of SVCs.

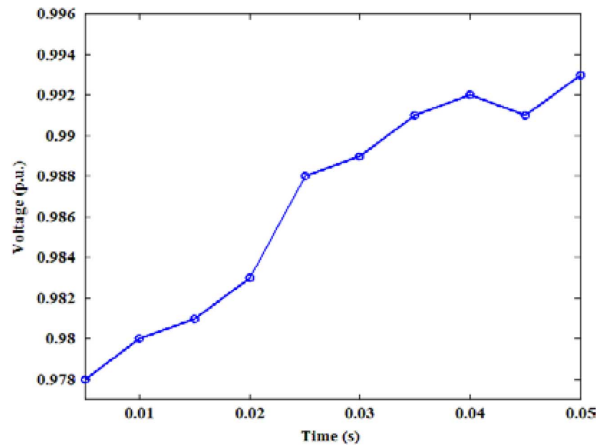

Fig. 17. Minimum voltage of the system.

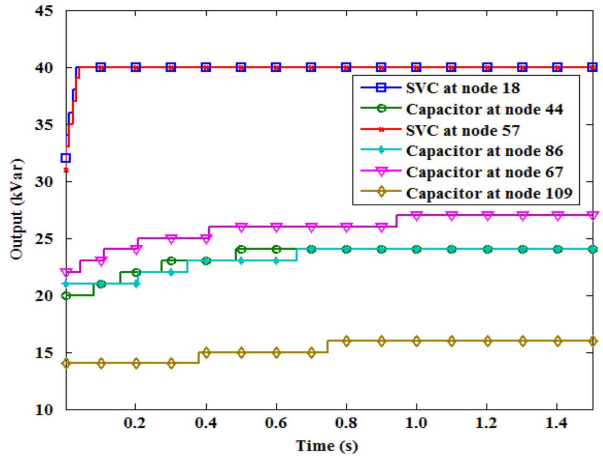

Fig. 18. Outputs of CBs and SVCs.

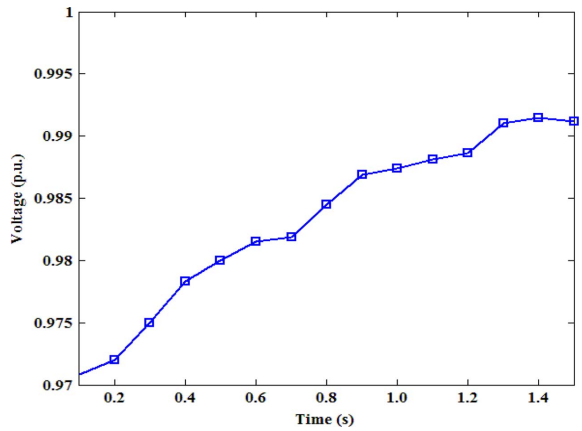

Fig. 19. Minimum voltage of the system.

two PV generators decrease from 400 kW to 200 kW. Fig. 18 shows the responses of the SVC and CBs. Fig. 19 shows the minimum voltage. It can be seen the minimum node voltage is within the range after 1.5 seconds, which shows the fast and effective voltage regulation of the proposed method during the transient cloud movement.

V. Conclusion

In this paper, a hybrid VVC control architecture is proposed for distribution systems with a high PV penetration. Coordinated control and local control are combined in this architecture for dispatching OLTC, SVCs and CBs. The paper assumes CBs and SVCs are already deployed before the implementation of the proposed VVC. When there is no cloud, the algorithm schedules hourly operation dispatches for VVC devices to minimize power losses and voltage deviations. When clouds move over, the local control loop becomes effective. To provide rapid response to PV output fluctuations due to transient cloud effects, SVCs and CBs are self-controlled without communication to regulate voltages at their installed nodes. SVCs will operate in the first stage. If voltage levels are still out of range, CBs will operate in the second stage. Time-adaptive delays are applied to CBs to prevent overcompensation. Simulation results show that the proposed algorithm can effectively reduce power losses and voltage deviations, while keeping the voltages at desired levels during cloud-moving periods.

Compared with previous VVC methods for circuits with a high PV penetration as mentioned in the introduction, the proposed hybrid architecture has notable advantages: 1) it does not require inverters to provide reactive power; 2) it is based on popular VVC devices; 3) it can optimize system operations and regulate voltages in cloudy periods. Thus, the proposed method is consistent with current PV integration standards and is more suitable as well as economical to be implemented in practice.

Appendix

Two-feeder test system

Bus No.	From Node	To Node	P_{Load} (kw)	Q_{Load} (kvar)	Length (km)
1	1	2	57.5	25.5	0.032
2	2	4	62.5	25	2.5
3	4	6	50	17	2.5
4	6	8	85.75	15.5	1.75
5	8	10	64.5	15	1.5
6	10	12	54	12.5	0.75
7	1	3	60	14.5	0.11
8	3	5	55	17.75	2.5
9	5	7	77	13	2.5
10	7	9	68	12	1.0
11	9	11	85.75	13	1.5
12	11	13	75.9	13	0.75

Substation voltage: 8kv, base MVA: 1.5 MVA, Resistance: $5\times10^{-2}\ \Omega/km$, Inductance: $4\times10^{-4}\ H/km$, Loads are connected at 'to nodes'.

ACKNOWLEDGMENT

The submitted manuscript has been created by UChicago Argonne, LLC, Operator of Argonne National Laboratory ("Argonne"). Argonne, a U.S. Department of Energy Office of Science Laboratory, is operated under Contract DE AC02-06CH11357. The U.S. Government retains for itself, and others acting on its behalf, a paid-up nonexclusive, irrevocable worldwide license in said article to reproduce, prepare derivative works, distribute copies to the public, and perform publicly and display publicly, by or on behalf of the Government.

REFERENCES

[1] F. A. Viawan and D. Karlsson, "Combined local and remote voltage and reactive power control in the presence of induction machine distributed generation," *IEEE Trans. Power Syst.*, vol. 22, pp. 2003–2012, 2007.

[2] R.-H. Liang and C.-K. Cheng, "Dispatch of main transformer ULTC and capacitors in a distribution system," *IEEE Trans. Power Del.*, vol. 16, pp. 625–630, 2001.

[3] J.-Y. Park, S.-R. Nam, and J.-K. Park, "Control of a ULTC considering the dispatch schedule of capacitors in a distribution system," *IEEE Trans. Power Syst.*, vol. 22, pp. 755–761, 2007.

[4] K. M. Son, K. S. Moon, S. K. Lee, and J. K. Park, "Coordination of an SVC with a ULTC reserving compensation margin for emergency control," *IEEE Trans. Power Del.*, vol. 15, pp. 1193–1198, 2000.

[5] Z. Wang and J. Wang, "Review on implementation and assessment of conservation voltage reduction," *IEEE Trans. Power Syst.*, vol. 29, pp. 1306–1315, 2014.

[6] Z. Wang, B. Chen, J. Wang, M. Begovic, D. Zhao, and L. Du, "MPC-based voltage/var optimization for distribution circuits with distributed generators and exponential load models," *IEEE Trans. Smart Grid*, to be published.

[7] S. Eftekharnejad, V. Vittal, G. T. Heydt, B. Keel, and J. Loehr, "Impact of increased penetration of photovoltaic generation on power systems," *IEEE Trans. Power Syst.*, vol. 28, pp. 893–901, 2013.

[8] Z. Wang, Q. Ai, D. Xie, and C. Jiang, "A research on shading and LCOE of building integrated photovoltaic," in *Proc. 2011 Asia-Pacific Power Energy Eng. Conf. (APPEEC)*, pp. 1–4.

[9] K. Turitsyn, P. Sulc, S. Backhaus, and M. Chertkov, "Distributed control of reactive power flow in a radial distribution circuit with high photovoltaic penetration," in *Proc. 2010 IEEE Power Energy Soc. Gen. Meet.*, pp. 1–6.

[10] T. Niknam, M. Zare, and J. Aghaei, "Scenario-based multiobjective volt/var control in distribution networks including renewable energy sources," *IEEE Trans. Power Del.*, vol. 27, pp. 2004–2019, 2012.

[11] D. Ton, C. Hanley, G. Peek, and J. D. Boyes, 2008, "Solar energy grid integration systems-energy storage (SEGIS-ES)," Available: [Online]. Available: http://www1.eere.energy.gov/solar/pdfs/segis-es_concept_paper.pdf

[12] R. Yan and T. K. Saha, "Investigation of voltage stability for residential customers due to high photovoltaic penetrations," *IEEE Trans. Power Syst.*, vol. 27, pp. 651–662, 2012.

[13] N. Kakimoto, H. Satoh, S. Takayama, and K. Nakamura, "Ramp-rate control of photovoltaic generator with electric double-layer capacitor," *IEEE Trans. Energy Convers.*, vol. 24, pp. 465–473, 2009.

[14] K. Turitsyn, P. Sulc, S. Backhaus, and M. Chertkov, "Options for control of reactive power by distributed photovoltaic generators," *Proc. IEEE*, vol. 99, pp. 1063–1073, 2011.

[15] P. Jahangiri and D. C. Aliprantis, "Distributed volt/var control by PV inverters," *IEEE Trans. Power Syst.*, vol. 28, no. 3, pp. 3429–3439 , Aug. 2013.

[16] M. Farivar, C. R. Clarke, S. H. Low, and K. M. Chandy, "Inverter VAR control for distribution systems with renewables," in *Proc. 2011 IEEE Int. Conf. Smart Grid Commun. (SmartGridComm)*, pp. 457–462.

[17] H.-G. Yeh, D. F. Gayme, and S. H. Low, "Adaptive VAR control for distribution circuits with photovoltaic generators," *IEEE Trans. Power Syst.*, vol. 27, pp. 1656–1663, 2012.

[18] B. A. Robbins, C. N. Hadjicostis, and A. D. Domínguez-García, "A two-stage distributed architecture for voltage control in power distribution systems," *IEEE Trans. Power Syst.*, vol. 28, no. 2, pp. 1470–1482, May 2013.

[19] D. L. Bassett, "Update of the status of IEEE 1547.8," in *Proc. 2012 IEEE PES Transm. Distrib. Conf. Expo. (T&D)*, pp. 1–3, expanding on IEEE Standard 1547.

[20] *IEEE Standard for Interconnecting Distributed Resources With Electric Power Systems*, IEEE Std. 1547-2003, 2003, pp. 0_1–16.

[21] H. Li, F. Li, Y. Xu, D. T. Rizy, and S. Adhikari, "Autonomous and adaptive voltage control using multiple distributed energy resources," *IEEE Trans. Power Syst.*, vol. 28, pp. 718–730, 2013.

[22] A. Maknouninejad, N. Kutkut, I. Batarseh, and Z. Qu, "Analysis and control of PV inverters operating in VAR mode at night," in *Proc. 2011 IEEE PES Innov. Smart Grid Technol. (ISGT)*, pp. 1–5.

[23] S. Kincic *et al.*, "Voltage support by distributed static VAr systems (SVS)," *IEEE Trans. Power Del.*, vol. 20, pp. 1541–1549, 2005.

[24] P. S. Sensarma, K. R. Padiyar, and V. Ramanarayanan, "Analysis and performance evaluation of a distribution STATCOM for compensating voltage fluctuations," *IEEE Trans. Power Del.*, vol. 16, pp. 259–264, 2001.

[25] W. Yang, Z. Peng, L. Wenyuan, X. Weidong, and A. Abdollahi, "Online overvoltage prevention control of photovoltaic generators in microgrids," *IEEE Trans. Smart Grid*, vol. 3, pp. 2071–2078, 2012.

[26] Y. Filion, A. Coutu, and R. Isbister, "Experience with controlled switching systems (CSS) used for shunt capacitor banks: Planning, studies and testing accordingly with CIGRE A3-07 working group guidelines," in *Proc. CIGRE/IEEE PES Int. Symp. Quality Security Elect. Power Del. Syst. (CIGRE/PES 2003)*, pp. 80–85.

[27] H. Stewardson, B. Novac, and I. Smith, "Fast exploding-foil switch techniques for capacitor bank and flux compressor output conditioning," *J. Phys. D, Appl. Phys.*, vol. 28, p. 2619, 1995.

[28] F. Ding, X. Duan, J. Zou, and M. Liao, "Controlled switching of shunt capacitor banks with vacuum circuit breaker," in *Proc. Int. Symp. Discharges Electr. Insul. Vacuum (ISDEIV'06)*, pp. 447–450.

[29] S. Jalali, I. Dobson, R. H. Lasseter, and G. Venkataramanan, "Switching time bifurcations in a thyristor controlled reactor," *IEEE Trans. Circuits Syst. I, Fundam. Theory Appl.*, vol. 43, pp. 209–218, 1996.

[30] M. E. Baran and F. F. Wu, "Network reconfiguration in distribution systems for loss reduction and load balancing," *IEEE Trans. Power Del.*, vol. 4, pp. 1401–1407, 1989.

[31] R. J. Koessler, "Dynamic simulation of static VAR compensators in distribution systems," *IEEE Trans. Power Syst.*, vol. 7, pp. 1285–1291, 1992.

[32] M. Baran and F. F. Wu, "Optimal sizing of capacitors placed on a radial distribution system," *IEEE Trans. Power Del.*, vol. 4, pp. 735–743, 1989.

[33] F. Milano, *Power System Modelling and Scripting*. New York: Springer, 2010.

[34] D. M. Divan, H. Chen, and A. Prasai, "Systems and methods for switch-controlled var sources coupled to a power grid," Application filed, with USPTO, Dec. 2012.

[35] M. Marwali, M. Haili, S. Shahidehpour, and K. Abdul-Rahman, "Short term generation scheduling in photovoltaic-utility grid with battery storage," *IEEE Trans. Power Syst.*, vol. 13, pp. 1057–1062, 1998.

[36] N. Daratha, B. Das, and J. Sharma, "Coordination between OLTC and SVC for voltage regulation in unbalanced distribution system distributed generation," *IEEE Trans. Power Syst.*, vol. 29, pp. 289–299, 2014.

[37] W. H. Kersting, "Radial distribution test feeders," *IEEE Trans. Power Syst.*, vol. 6, pp. 975–985, 1991.

Zhaoyu Wang (S'13) received the B.S. degree in electrical engineering from Shanghai Jiaotong University, Shanghai, China, in 2009, the M.S. degree in electrical engineering from Shanghai Jiaotong University in 2012, and the M.S. degree in electrical and computer engineering from the Georgia Institute of Technology, Atlanta, GA, USA, in 2012. He is now working towards the Ph.D. degree in the School of Electrical and Computer Engineering, Georgia Institute of Technology. In 2013, he worked as a research aide intern at Decision and Information Sciences Division, Argonne National Laboratory, Argonne, IL, USA. His current research interests include microgrids, volt/var control, demand response and conservation, system modeling and identification, stochastic optimization in power systems.

Hao Chen received the B.S. degree in electrical engineering from Nanjing University of Science & Technology, Nanjing, China, in 2007, and the M.S. degree in electrical engineering from Illinois Institute of Technology, Chicago, IL, USA, in 2010. From 2010 to 2012, he was an electrical engineer at Varentec, San Jose, CA, USA. He is currently working toward the Ph.D. degree of electrical engineering at the Georgia Institute of Technology, Atlanta, GA, USA. His research focus is power electronics applications in smart grid.

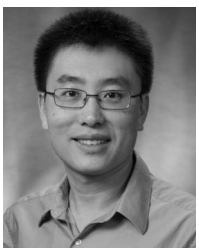

Jianhui Wang (M'07–SM'12) received the Ph.D. degree in electrical engineering from Illinois Institute of Technology, Chicago, IL, USA, in 2007.

Presently, he is a Computational Engineer with the Decision and Information Sciences Division at Argonne National Laboratory, Argonne, IL, USA.

Dr. Wang is the chair of the IEEE Power & Energy Society (PES) power system operation methods subcommittee. He is an Editor of the IEEE TRANSACTIONS ON POWER SYSTEMS, the IEEE TRANSACTIONS ON SMART GRID, an Associate Editor of *Journal of Energy Engineering*, an Editor of the IEEE *PES Letters*, and an Associate Editor of *Applied Energy*. He is also an Affiliate Professor at Auburn University, Auburn, AL, USA, and an adjunct professor at University of Notre Dame, South Bend, IN, USA.

Miroslav M. Begovic (S'87–M'89–SM'92–F'04) is Professor and Chair of the Electric Energy Technical Interest Group in the School of Electrical Engineering at Georgia Institute of Technology. His studies focus on analysis, monitoring, and control of voltage stability and applications of phasor measurements in electrical power systems. His research is concentrated on real-time monitoring systems for control of power system dynamics, protective relaying, distribution network operation, and distributed resources in energy systems. A member of IEEE PES Power System Relaying Committee, Dr. Begovic is a former Chair of the IEEE PES Emerging Technologies Coordinating Committee and has contributed to technical activities within IEEE and CIGRE. Dr. Begovic is a member of Sigma Xi, Tau Beta Pi, Phi Kappa Phi, and Eta Kappa Nu and currently serves as President of IEEE Power and Energy Society.